TABLE 1 Comparison of X-band LNAs in 0.18-μm CMOS

Ref.	*f*o (GHz)	PDC (mW)	Gain (dB)	R.L. (dB)	NF (dB)	Pin-1dB (dBm)	IIP3 (dBm)	Gain (dB)/mW	Chip area (mm^2)	Architecture
[2]	10.8	17.6	9	>10	2.5	+2.5	+4.1	0.51	0.46	Cascode parallel resonant
[3]	9	15	16.5	>7	4.5	−15	NA	1.1	0.38	Cascode with gain-enhanced inductor
[4]	9	19.6	12.2	>5	3.7	−8.7	NA	0.62	0.9	Folded cascode
[7]	10	13.7	10	>10	4.5	−15	−6	0.73	0.8	Dual FET single stage
[8]	11	50.4	12	>15	3.5	−8.5	5	0.24	0.48	Cascade two stage
This Work	10.7	5.5	20.4	>11	3.7	−32	−18.3	3.7	0.59	Cascade CR

metal layer and are realized in octagonal forms for minimizing resistive losses. Figure 3 shows the chip photo of the fabricated CR-LNA with a chip area of 0.59 mm^2 including all testing pads. Note that the 15-pF capacitor (C_3) is implemented by an array of capacitors, and it consumes about 120 × 180 μm^2 chip area.

The CR-LNA consumes 5.5 mW from a 1.3-V supply voltage, and undesired parasitics of pads and interconnections are removed by a de-embedding procedure. The measurement results of *S*-parameters and NF is shown in Figure 4(a). The good agreement between measured and simulated results is also observed. The measured small signal gain ($|S_{21}|$) and NF is 20.4 and 3.7 dB at 10.7 GHz, respectively. Moreover, the measured input return loss ($|S_{11}|$) and output return loss ($|S_{22}|$) is about 11 and 18 dB at 10.7 GHz. Figure 4(b) shows the measured input P_{1dB} and the third-order nonlinearity (IIP3) of the CR-LNA. One tone at 10.7 GHz was applied to the input P1dB measurement, and two tones were applied to the IIP3 measurement with equal power level at 10.7 and 10.8 GHz. The measured input P1dB and IIP3 is −32 and −18.3 dBm. Table 1 summarizes previously reported 18-μm CMOS LNAs at X-band, and this work demonstrates the highest gain performance with the lowest power consumption.

4. CONCLUSION

In this article, a novel design of the X-band CR-LNA with high-gain performance and low-power consumption is presented. The CR-LNA has successfully implemented, measured, and verified with superior performances. The gain enhancement is realized by the three CS cascade amplifiers, and the power consumption is economized by the CR topology. Compared to previously reported 0.18-μm CMOS LNAs at X-band, the presented design achieves the highest gain performance while maintains the lowest power consumption. It is convinced that the proposed design methodology reveals great potentials for X-band radar or other wireless communication applications.

ACKNOWLEDGMENT

The authors would like to thank the National Science Council (NSC) and Chip Implementation Chip (CIC) of Taiwan for financial and technical supports. This work was supported by the NSC under Contract NSC-100-2221-E-027-088.

REFERENCES

1. J. Gil, K. Han, and H. Shin, 13 GHz 4.67 dB NF CMOS low-noise amplifier, Electron Lett 39 (2003), 1056–1058.
2. K.J. Sun, Z.M. Tsai, K.Y. Lin, and H. Wang, A 10.8-GHz CMOS low-noise amplifier using parallel-resonant inductor, In: International Microwave Symposium Digest, Honolulu, HI, 2007, pp. 1795–1798.
3. S. Wang, Design of a 9 GHz CMOS low noise amplifier using gain-enhanced technique, Microwave Opt Tech Lett 53 (2011), 479–481.
4. T.K.K. Tsang and M.N. El-Gamal, Gain controllable a very low voltage (<1 V) 8–9 GHz integrated CMOS LNAs," In: IEEE RFIC Symposium Digest, Seattle, WA, 2002, pp. 205–208.
5. C.H. Liao and H.R. Chuang, A 5.7-GHz 0.18-p.m CMOS gain-controlled differential LNA with current reuse for WLAN receiver, IEEE Microwave Wireless Compon Lett 13 (2003), 526–528.
6. H.H. Hsieh and L.H. Lu, Design of ultra-low-voltage RF frontends with complementary current-reused architectures, IEEE Trans Microwave Theory Tech 55 (2007), 1445–1458.
7. C.L. Yang, T.H. Hsieh, and Y.C. Chiang, A novel self-biased low noise amplifier with current-reused technique for *X* band applications, In: Asia-Pacific Microwave Conference Digest, Singapore, 2009, pp. 1667–1670.
8. B. Afshar and A.M. Niknejad, X/*Ku* band CMOS LNA design technique," in Proc IEEE CICC Conference Digest, 2006, pp. 389–392.

PHASE-LOCKED HOMODYNE MEASUREMENT OF QUASIPROBABILITY Q FUNCTION AND DETECTION OF INFORMATION-CARRYING WEAK-COHERENT STATES

Edith Garcia,[1] Francisco J. Mendieta,[2] Josue A. Lopez,[3] Eduardo Alvarez,[1] Arturo Arvizu,[3] and Philippe Gallion[4]

[1] Universidad Autónoma de Baja California, Tijuana, BC 22426, México; Corresponding author: egarcia@uabc.edu.mx

[2] Agencia Espacial Mexicana, Xola y Universidad, D.F., CP 03020, México

[3] CICESE, Ensenada, BC 22860, México

[4] Ecole Nationale Supérieure des Télécommunications, Telecom-ParisTech, CNRS LTCI UMR 5141, 46 rue Barrault, Paris 75013, France

Received 28 February 2013

ABSTRACT: *We present an eight-port homodyne receiver implemented in free space technology for detection of weak coherent states that carry binary information. For transmitted power economy, we use suppressed-carrier modulation, therefore, we have implemented an optical Costas-loop-type carrier synchronizer. We obtain the quasiprobability Q function from the in-phase and quadrature observables that are simultaneously measured. Statistical results for the quadrature components are presented. We perform measurements for the bit error rate and the mutual information between transmitter–receiver. The results show that the proposed setup is suitable in quantum communications and continuous variable quantum key distribution systems.* © 2013 Wiley Periodicals, Inc.

Microwave Opt Technol Lett 55:2431–2437, 2013; View this article online at wileyonlinelibrary.com. DOI 10.1002/mop.27844

Key words: *Q function measurement; weak coherent states; quantum key distribution; eight-port homodyne detector; optical Costas loop*

1. INTRODUCTION

In the current world with globalized economy, confidential and secure communications are mandatory. Therefore, several research centers have increased their efforts to produce technological advances, capable to offer increasing security levels for the information to be transmitted [1,2]. One of such technologies is the quantum cryptography, based for instance on the Bennet–Brassard protocol proposed in 1984, and usually referred as BB84 [3]. This protocol makes use of quantum mechanics principles such as quantum demolition measurements, and the noncloning theorem, for the transmission of the cryptographic key, referred as quantum key distribution (QKD). This scheme does not depend on computational algorithms, but on the quantum properties of the photons used for the key distribution, offering unconditional security. Among some proposals for the QKD receivers, there is the one based in photon counters; where the information is transmitted by manipulation of a single photon's properties, which implies the use of single-photon sources and detectors; however, this detectors exhibit low quantum efficiency at the telecommunications wavelengths, besides working in Geiger mode requiring quenching; as a result the detector is limited to data rates up to 8 Mbps [4–6], which is a very low speed as compared to the requirements of present and future networks.

Other proposed techniques for the QKD make use of efficient modulation systems such as phase shift keying (PSK) on continuous variables (CV) with homodyne balanced detection [7–9]. In this article, we present a modulation and detection system for a CV system with weak-coherent-states (WCS), as an alternative to a single photon source systems. We first measure the quasiprobability function of the received field and then, we proceed to the detection of its quadratures. In this setup, we use a strong local oscillator (LO) and at the receiver system, PIN balanced photo detectors are used, these detectors present high quantum efficiency at room temperature at the wavelengths used in current optical communications networks [10], so this proposal presents the capability of higher QKD rates. Our systems consist of an eight-port homodyne receiver, therefore, the zero-point fluctuation noise is considered at each, eventually used, receiver input to take into account the excess of noise due to the simultaneous quadrature measurement of the optical field. For transmitted power economy, we use suppressed carrier modulation, so we had to implement an optical Costas loop-type subsystem in order to phase-lock both the signal and the LO phases.

The system is implemented in a free-space scheme at the 1550-nm wavelength used in telecommunication systems. The cryptographic symbol rate is 350 kbps with a suppressed-carrier binary phase shift keying modulation scheme (BPSK). The received signals are statistically postprocessed in order to show that this setup has the ability to discriminate the electric levels for the logical "1"s and "0"s, down to an average signal level of 0.25 photon per bit. We measure the quasiprobability $\boldsymbol{Q}$ function of the received field directly, we measure the uncertainty relationship for the quadratures I and Q measured and experimentally verify that it complies with the relationship for the simultaneous quadratures measurement of the optical field. The bit error rate (BER) and the mutual information (I) between Alice and Bob (I_{AB}) are finally obtained.

2. THEORY

Figure 1 shows the block diagram of our eight-port hybrid setup where the optical signals E_{LO} (LO) and E_{sig} (WCS-signal) carrying the transmitter data are mixed. Both noise free signals are described classically below by Eqs. (1) and (2), respectively.

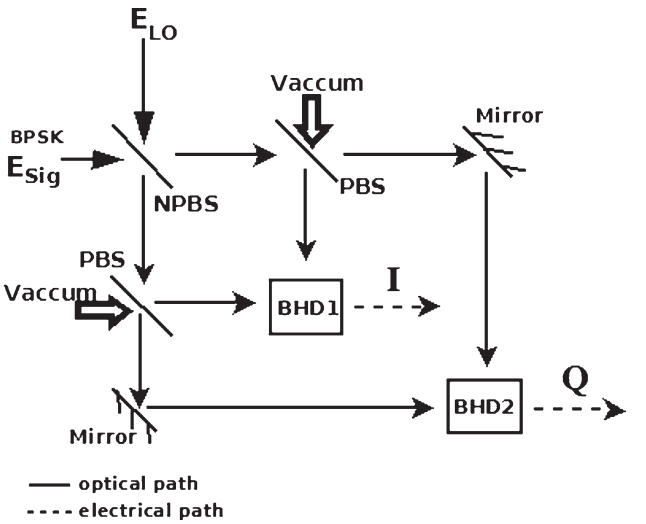

Figure 1 Block diagram of the eight-port hybrid for simultaneous measurement of the quadratures of optical field in free space with weak coherent states. BHD1: Balanced photo detector 1, BHD2: Balanced photo detector 2, PBS: Polarized beam splitter, NPBS: Non polarized beam splitter

$$E_{\text{sig}} = \sqrt{P_{\text{sig}}}\, e^{j(\omega_c t+\theta)}, \tag{1}$$

$$E_{\text{LO}} = \sqrt{P_{\text{LO}}}\, e^{j\omega_{\text{LO}} t}, \tag{2}$$

where P_{sig} is the information signal power, θ is the relative modulated phase signal, P_{LO} is the LO power, ω_c is the angular frequency of the data signal, and ω_{LO} is the angular frequency of the LO signal. In this setup, the frequencies of the signal and LO at the input of the homodyne receiver are identical as we use a homodyne configuration. E_{sig} and E_{LO} are introduced into the eight-port system and are mixed in an optical beam splitter (BS); therefore, the output signal power can be expressed as:

$$P(t) = \frac{1}{2}|E_{\text{sig}} + E_{\text{LO}}|^2. \tag{3}$$

The beat signal is split in its two orthogonal linear components through polarized beam splitters (PBS). In this way, it is possible to detect the in-phase (I) (at the first balanced homodyne detector: BHD1) and the quadrature (Q) components (at the second balanced homodyne detector: BHD2). In both quadratures there exist both the classical term (average value of the observable) and the quantum term (random fluctuations around the average) that are described through the photon number in the Eqs. (4) and (5), where $\hat{N}$ is the quantum number operator [11]

$$I = \hat{N}_{\text{InPhase}} + \Delta\hat{N}_{\text{InPhase}} \tag{4}$$

$$Q = \hat{N}_{\text{Quadrature}} + \Delta\hat{N}_{\text{Quadrature}} \tag{5}$$

where $\langle\hat{N}\rangle$ and $\langle\Delta\hat{N}\rangle$ are the average signal photon number and the average photon number fluctuations, respectively.

In our scheme, we used linear polarization at 45° for the signal field and circular polarization for the LO, therefore, the LO beats with the I component at the BHD1 and with the Q

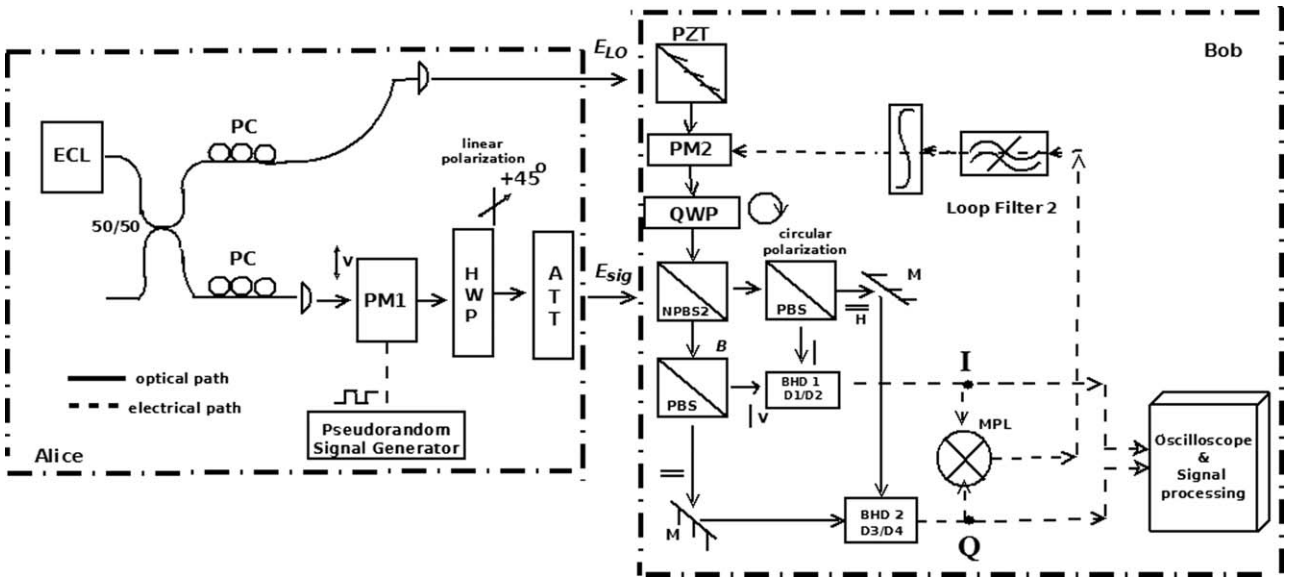

Figure 2 Experimental set up of the eight-port homodyne receiver with the feedback system based on the Costas loop with BPSK modulation for WCS in free space and balanced photodetection. ECL: External cavity laser, PM: Phase modulator, PC: Polarization controller, NPBS: Non polarized beam splitter, PBS: Polarized beam splitter, HWP: Half wave plate, QWP: Quarter wave plate, ND: Neutral density filter, BHD: Balanced homodyne detector, PZT: Piezoelectric, MPL: Multiplier, M: Mirror, ATT: Attenuator

component at the BHD2. Taking into account Eqs. (1) through (3), and the responsivity R of the balanced photoreceiver, the current i_{ph} produced can be found, for each BHD as

$$i_{\mathrm{ph}_I}(t)=2R\sqrt{P_{\mathrm{sig}}P_{\mathrm{LO}}}\cos\left(\theta(t)+\Delta\theta\right), \tag{6}$$

$$i_{\mathrm{ph}_Q}(t)=2R\sqrt{P_{\mathrm{sig}}P_{\mathrm{LO}}}\sin\left(\theta(t)+\Delta\theta\right) \tag{7}$$

which represent the electric current produced by the impinging photon flows and can be directly linked to the received optical power. As the system has a homodyne configuration, the measured variations will depend only on the phase difference between the LO and the BPSK data signal. $\Delta\theta$ is the phase difference between E_{sig} and E_{LO}, which will be forced to zero by our optical-Costas-loop.

From the expressions of I and Q, it is possible to calculate the quasiprobability distribution of the observables according to the **Q** function equation as follows: First the Wigner quasiprobability distribution for a coherent state signal [Eq. (8)] is convolved with a Gaussian distribution that represents the vacuum state [12], to yield the quasiprobability (Husimi) **Q** function [Eq. (9)]:

$$W(I,Q)=\frac{1}{\pi}e^{\left[-(I-I_0)^2-(Q-Q_0)\right]^2} \tag{8}$$

$$\mathbf{Q}(I,Q)=\frac{1}{2\pi}e^{\left[-\frac{1}{2}(I-I_0)^2-\frac{1}{2}(Q-Q_0)\right]^2} \tag{9}$$

where $(I-I_0)$ is the coherent quantum state of the observable (I) displaced from the vacuum state (I_0).

As it is known, the results from measurements are not 100% efficient, as in the case of our setup where we have an overall quantum efficiency $\eta=0.7$, as we will discuss in section 3.

In our system, with BPSK modulation and simultaneous quadrature measurement, the signal to noise ratio (SNR) and the BER can be expressed as a function of the photon number by the Eqs. (10) and (11):

$$SNR=\frac{\langle\hat{N}_{\mathrm{InPhase}}\rangle^2}{\langle\hat{N}^2_{\mathrm{InPhase}}\rangle}=2N \tag{10}$$

$$BER=\frac{1}{2}erfc\sqrt{N} \tag{11}$$

where N is the average photon number per bit [13–15] and *erfc* is the complementary error function. Equations (10) and (11) correspond to the simultaneous quadrature measurement, for which the SNR doubles with respect to the single quadrature measurement (with single BHD detection), where we have,

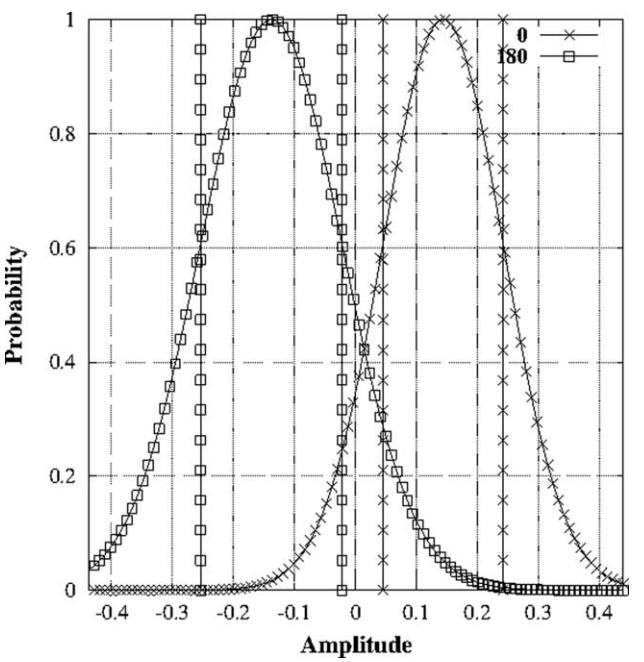

Figure 3 Histograms for the logical levels 1's and 0's of the received data (I), for $N=1$ photon average per bit

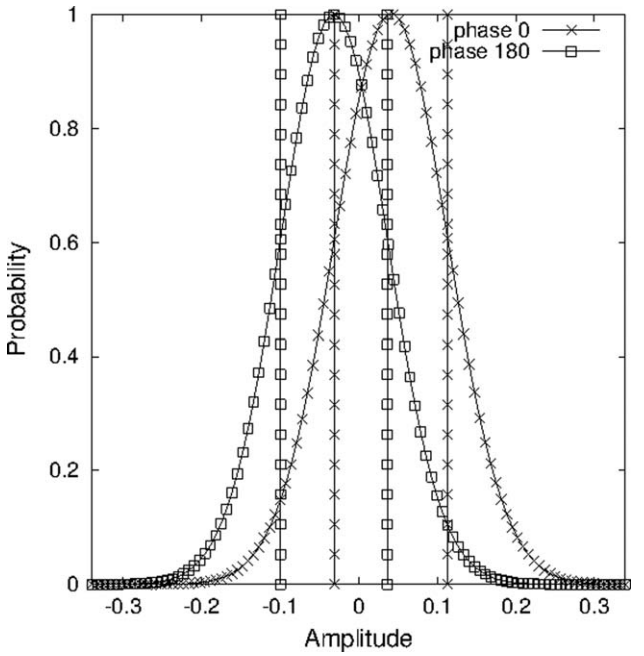

Figure 4 Histograms for the logical level 1's and 0's of the received data (I), for $N = 0.25$ photon average per bit

respectively, $SNR = 4N$ and $BER = \frac{1}{2} erfc\sqrt{2N}$ [13]. Now, coming back to our case of simultaneous quadrature measurement, the probability density distribution for this signal is calculated through the following Eqs. (12) and (13):

$$P_e(I) = \sqrt{\frac{1}{2\pi}} \exp\left[\frac{-1}{2}\left(\hat{N}_{\text{InPhase}} + \Delta\hat{N}_{\text{InPhase}}\right)^2\right] \tag{12}$$

$$P_e(Q) = \sqrt{\frac{1}{2\pi}} \exp\left[\frac{-1}{2}\left(\hat{N}_{\text{Quadrature}} + \Delta\hat{N}_{\text{Quadrature}}\right)^2\right] \tag{13}$$

In a communication system, the most important aim is to approach the channel capacity, that is the maximization of the mutual information between Alice and Bob (I_{AB}), therefore, its calculation was done using the Shannon's equation [Eq. (14)] [15] for three conditions (a) ideal conditions (a lossless system), (b) theoretical conditions (taking into account the coupling losses, and attenuations that give us a 0.7 efficiency) and finally, (c) calculations with the experimental data results. In this experiment with BPSK modulation, the signal in-phase quadrature (I) constitutes the output signal with the received data, whereas the quadrature signal Q provides the required feedback loop signal in the system. For the I_{AB}, we only considered the error probability $P_e(I)$ of the data in the in-phase observable (I).

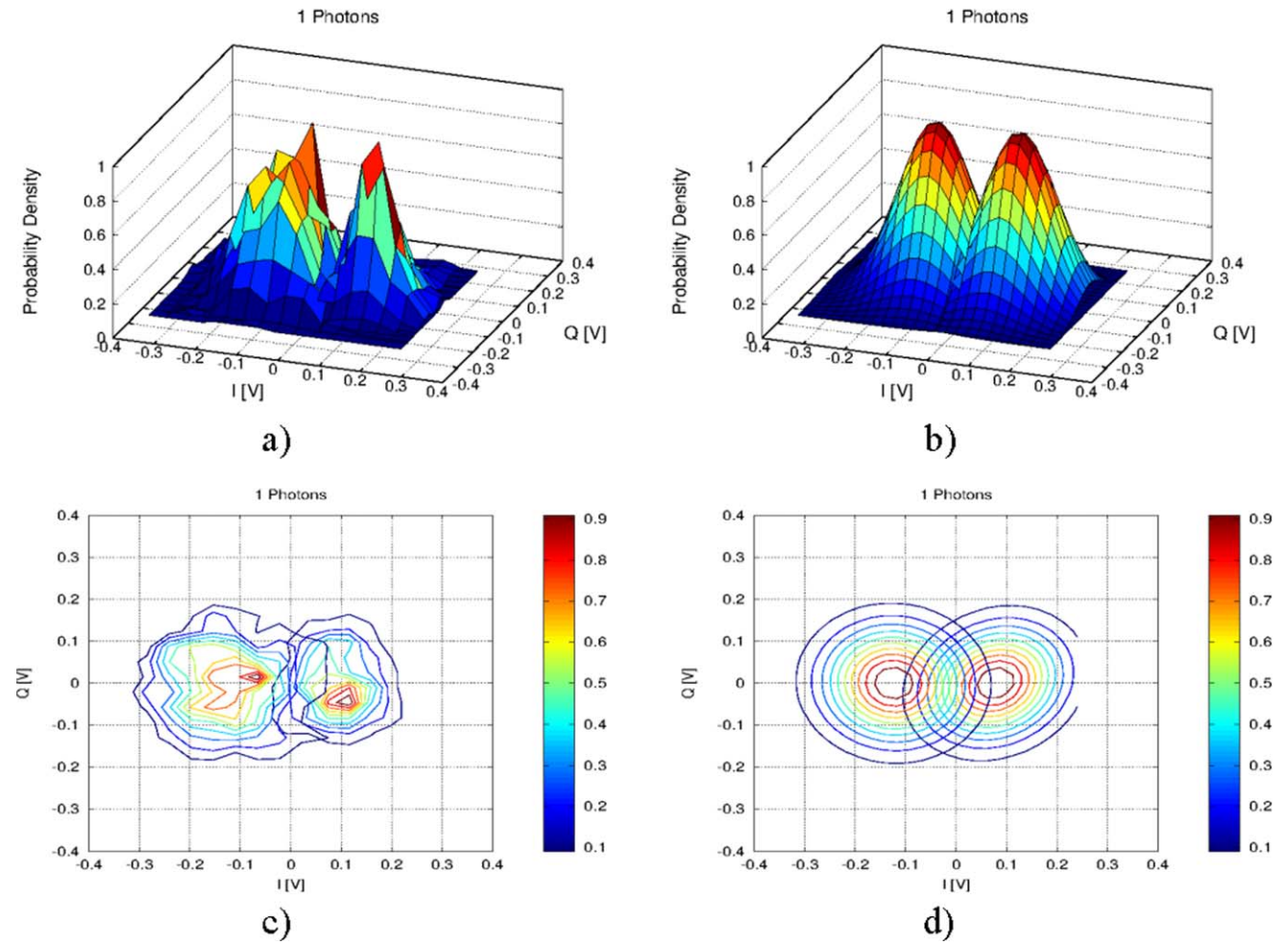

Figure 5 Results for 1 photon per bit. (a) Quasiprobability distribution **Q** function expression using the raw data, (b) reconstructed quasiprobability distribution using the mean and variance obtained from the raw data, (c) contour lines using the raw data, and (d) contour lines from the reconstructed distribution. [Color figure can be viewed in the online issue, which is available at wileyonlinelibrary.com]

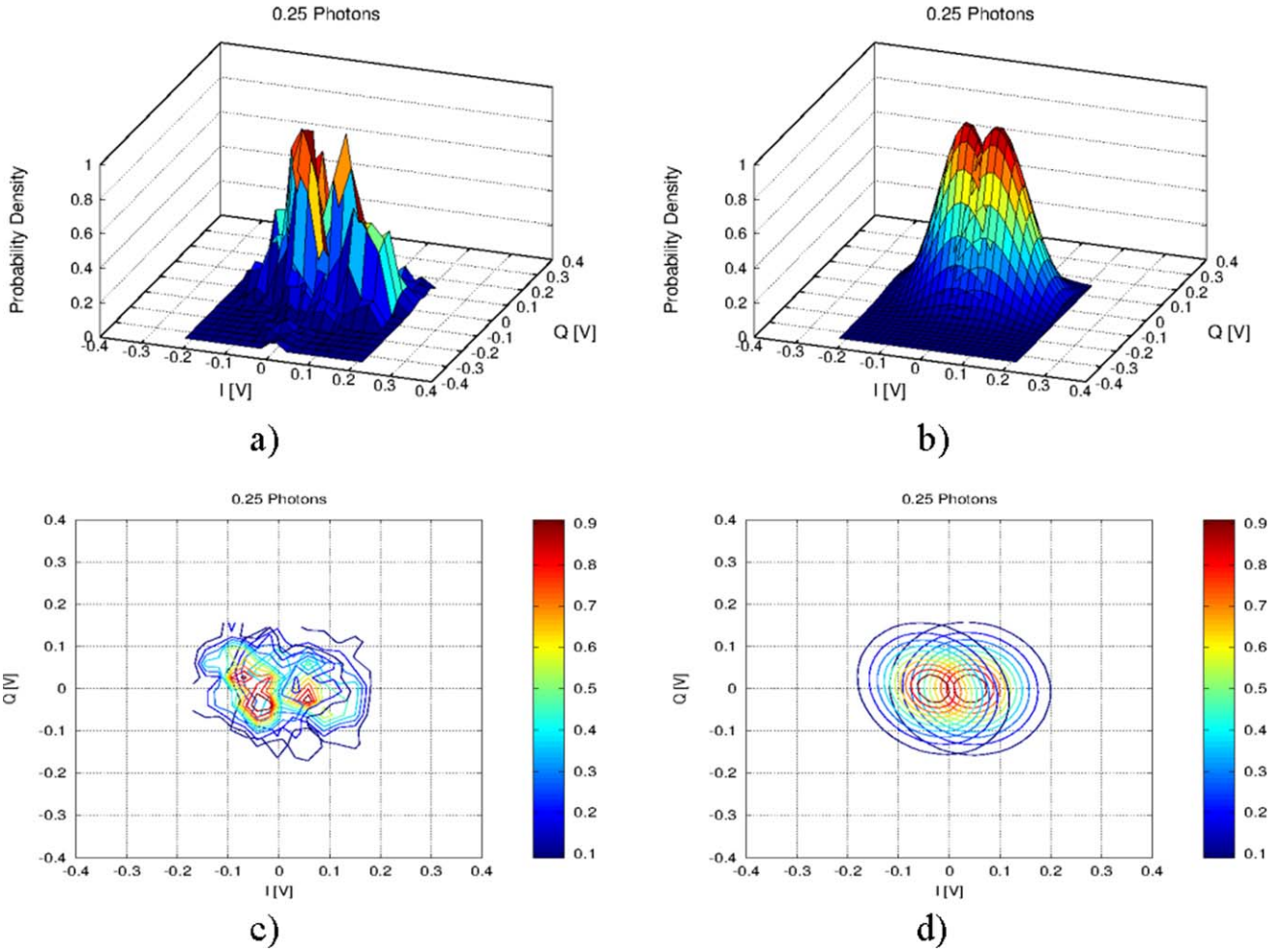

Figure 6 Results for 0.25 photon per bit. (a) Quasiprobability distribution **Q** function expression using the raw data (b) reconstructed quasiprobability distribution using the mean and variance obtained from the raw data, (c) contour lines using the raw data, and (d) contour lines from the reconstructed distribution. [Color figure can be viewed in the online issue, which is available at wileyonlinelibrary.com]

$$I_{AB} = 1 + P_e(I)\log_2 P_e(I) + (1 - P_e(I))\log_2(1 - P_e(I)) \quad (14)$$

As it is shown in the Figure 1, in this experiment the observables I and Q were measured simultaneously, so that there are two unused ports from where the vacuum noise enters into the system. As a result, there is an increase in the quantum noise (compared to a single quadrature or a commuted quadratures scheme) which is reflected as a fluctuation of $\Delta I = \Delta Q = h\nu$. The uncertainty relationship for this case is represented according to Eq. (15)

$$\langle I^2 \rangle \langle Q^2 \rangle \geq 1 \quad (15)$$

3. EXPERIMENTAL SETUP

As it is shown in Figure 2, the experimental setup consists of a free space eight-port interferometer, where we use an external cavity laser tuned to a 1550.1-nm wavelength. This laser is used both as the carrier for the data, and the LO in order to operate in an stabilization free self-homodyne configuration, thus simplifying the automatic frequency control, leaving only the optical phase lock to be implemented. A pseudorandom data sequence at 350 Kbps is generated and used to drive the electro-optical phase modulator PM1 in order to get the optical BSPK modulation.

In this setup, it is required to have well-defined polarization states that allow the detection of the conjugate variables at the BHD's. After setting the state of polarization of the modulated beam at a linear 45° polarization, the beam is attenuated by 120 dB through a set of calibrated neutral density filters in order to produce a quantum level signal, that is an optical beam power equivalent to 1 photon per bit duration; which in our case corresponds to a 45-fW signal power. This weak coherent signal is fed to the eight-port system. The LO signal (with a 2-mW power level) travels to a second phase modulator that will be used to control the relative LO phase in a feedback loop (Costas loop) to maintain the eight-port interferometer in-phase lock. Then a $\lambda/4$ polarizer (quarter wave plate) is used to produce a circular polarization state.

At the eight-port inputs, the LO and the weak power modulated beams are combined through a nonpolarized beam splitter, then the combined signals emerging from the BS are split in their vertical and horizontal components, using PBS. The vacuum noises enter in the system through the used and unused ports of the PBSs.

The vertical and horizontal optical fields impinge on the balanced homodyne detectors (BHD1 and BHD2), respectively. The electrical signals of the BHD's that correspond to the I and Q signals are simultaneously measured and they are postprocessed. The I and Q signals will be used to generate the

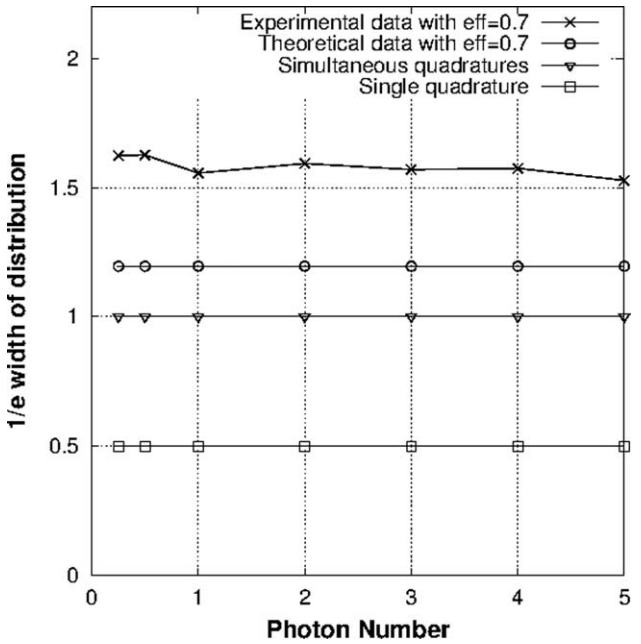

Figure 7 1/e width of distribution as a function of the photon number for (a) single quadrature measurements, (b) simultaneous quadratures measurements, (c) theoretical results for our setup with efficiency of $\eta = 0.7$ y, and (d) experimental results with efficiency of $\eta = 0.7$

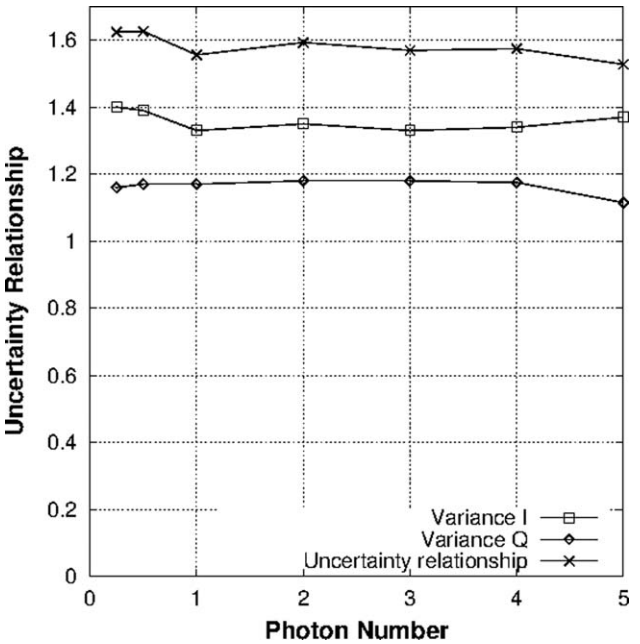

Figure 8 Uncertainty relationship for the quadratures I and Q as a function of the photon number

required error signals for the Costas loop that will enable phase locking between the data signal and the LO.

For information-carrying signals, a precise phase lock between the signal and the LO is required. As we are using an interferometric scheme we do not have a true optical voltage controlled oscillator (VCO) to get such phase lock; however, we implemented an "equivalent" optical VCO by means of the LO signal and an optical phase modulator driven by a signal obtained from processing the I and Q signals. Therefore, there is no need for a learning synchronizing sequence or residual carrier, which is of utmost importance in synchronous quantum communications and synchronous quantum cryptography. Our overall quantum efficiency is $\sim$0.7 due to optical losses and residual spatial mode mismatch between the signal and the LO.

4. EXPERIMENTAL RESULTS

Several measurements of I and Q quadratures for the WCS signals were made; for a data signal field with 0.25, 0.5, 1, 2, 3, 4, and 5 average photons per bit, modulated in BPSK with a pseudorandom data sequence. The histograms in Figures 3 and 4 show the distribution for the logical 1 and 0, obtained after a postdetection processing, for $N = 1$ and $N = 0.25$, respectively.

Figure 3 (1 average photon per bit), shows the statistical distribution of the measured data for the voltage produced by the logical levels 1 and 0, received in the BHD, there is a small overlapping zone, allowing a clear discrimination between the two logical levels. However, in Figure 4 ($N = 0.25$ average photons per bit duration), the overlapping between the symbols probability curves surpasses the first standard deviation, as a result we have an increase in the BER.

Figures 5 and 6 show the measured quasiprobability distributions and the contour lines for the experimental data for the case of 1 and 0.25 photons, respectively, for both the raw data (a and c) and the reconstructed distribution with the mean and variance obtained from the raw data (b and d). In the case of the contour line graphs, there is a slight asymmetry in one of the probability distributions; we attribute this to a slight unbalance in the input of the photo detectors, and/or due to the asymmetric modulation at the transmitter.

Figure 7 shows the value of the standard deviation of the probability distribution of the quadratures as a function of photon number for the following cases: (a) measurement of the single quadrature, (b) simultaneous measurement of quadratures, (c) theoretical result for our setup with efficiency $\eta = 0.7$, (d) experimental results with efficiency $\eta = 0.7$. Figure 8 shows the graph of the corresponding uncertainty relationship for $\langle I^2 \rangle \langle Q^2 \rangle > 1$.

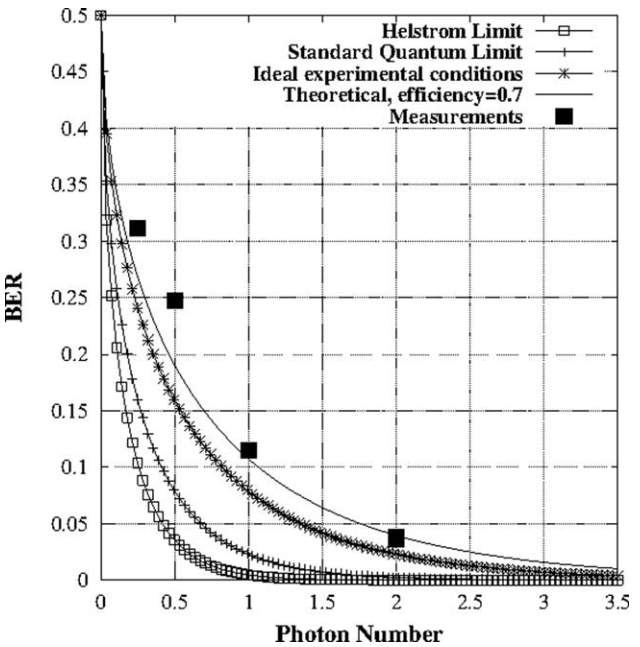

Figure 9 BER for different photons number, (a) Helstrom limit, (b) Standard quantum limit, (c) ideal experimental conditions, (d) theoretical conditions with $\eta = 0.7$, and (e) measured data

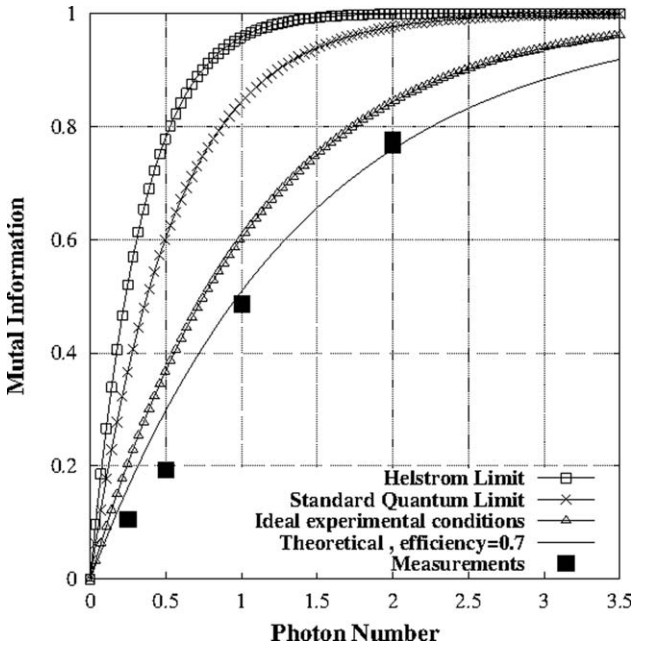

Figure 10 Mutual information between Alice and Bob for different values of photon number experiment, (a) Helstrom limit, (b) standard quantum limit, (c) ideal experimental conditions, (d) theoretical conditions with $\eta = 0.7$, and (e) measured data

In Figure 9, the theoretical and experimental BER results are compared, showing in general a good agreement, for our efficiency of 0.7. The Helstrom and standard quantum limits are also included for comparison [16].

Based on the measured BER, it is possible to calculate the mutual information achievable between Alice and Bob. The mutual information is calculated with the measured data. Figure 10 shows the mutual information results as compared with the theoretical values for 0.7 efficiency.

5. CONCLUSION

We report the theory and experimental demonstration of an eight-port optical hybrid receiver for high sensitivity detection of weak coherent signals, using a Costas loop-type synchronizer in order to perform measurements with information-carrying fields.

Our system allows the direct measurement of the quantum quasiprobability **Q** function as the two fields quadratures are measured simultaneously. The direct measurement of the quasiprobability function is interesting as compared to the standard tomography: although the latter yields the Wigner distribution, it requires the sweeping of the LO phase. Our system yields the **Q** function directly including the unavoidable additional noise due the simultaneous quadrature measurement, which is of interest for information-carrying fields.

The required phase lock is provided by the processing of the suppressed carrier WCS itself, therefore, there is no need for references for synchronization or residual carrier, which is of great importance in low-cost communications and in quantum cryptography.

Our system works with binary PSK modulation but it can be easily generalized to provide **Q** function measurement for higher-order modulation formats. Our experimental setup exhibits an acceptable optical efficiency and our BER, mutual information and uncertainty measurements are close to the predicted theoretical results.

The simultaneous quadrature measurement in our system is based on a polarization splitting of the signal in order to separate its quadratures, beating with a circularly polarized LO, thus providing the 0° and 90° references in a very stable setup with no need for compensation.

Finally, our system uses uncooled, high bandwidth and low cost standard PIN detectors, which is of great interest in quantum communications and quantum cryptography with CV operating at telecommunications wavelengths.

ACKNOWLEDGMENTS

This work has been supported by CONACYT-México; the authors thank M.C. Ramón Muraoka E. and M.C. Juan Carlos Domínguez V. for their technical support in the experimental setup.

REFERENCES

1. N. Gisin, G. Ribordy,W. Tittel, and H. Zbinden, Quantum cryptography, Rev Mod Opt 74 (2002), 145–195.
2. D. Stebila, M. Mosca, and N. Lutkenhaus, The case for quantum key distribution, In: Quantum Comm. 2009 Workshop on Quantum and Classical Information Security, Vico Equense, Italy, October 26, 2009.
3. C.H. Bennett and G. Brassard, Quantum cryptography: Public key distribution and coin tossing, In: International Conference on Computers, Systems and Signal Processing, Bangalore, India, December 10–12, 1984.
4. S. Cova, M. Ghioni, A. Lacaita, C. Samori, and F. Zappa, Avalanche photodiodes and quenching circuits for single-photon detection, Appl Opt 35 (1996), 1956–1976.
5. R.H. Hadfield, Single-photon detectors for optical quantum information applications, Nat photonics (2009), 696–705.
6. Q. Xu, M. Sabban, and P. Gallion, Homodyne detection of weak coherent optical pulse: Applications to quantum cryptography, Microwave Opt Technol Lett 51 (2009), 1934–1939.
7. T. Symul, V. Sharma, T.C. Ralph, and P.K. Lam, Coherent state quantum key distribution with continuous-wave laser beams, In: OSA/OFC/NFOEC, OWC6, San Diego, CA, March 2010.
8. F. Grosshans, G. Van Assche, J. Wenger, R. Brouri, N.J. Cerf, and P. Grangier, Quantum key distribution using gaussian-modulated coherent states, Nature 421 (2003), 238–241.
9. Y.M. Chi, B. Qi, W. Zhu, L. Qian, H.K. Lo, S.H. Youn, A.I. Lvovsky, and L. Tian, A balanced homodyne detector for high-rate Gaussian-modulated coherent-state quantum key distribution, New J Phys 13 (2011).
10. M. Navascués and A. Acín, Security bounds for continuous variables quantum key distribution, Phys Rev Lett 94 (2005), 020505 1–020505 4.
11. P. Gallion, F.J. Mendieta, and S. Jiang, Noise in optical communications and cryptography, Cap 3, In: E. Wolf (Ed.), Progress in optics, Vol. 52, Elsevier, Hungary, 2009, pp. 149–259.
12. L. Ulf, Measuring the quantum state of light, Cambridge University Press, Cambridge, UK, New York, 1997, pp. 193.
13. Q. Xu, A. Arvizu, P. Gallion, and F.J. Mendieta, Homodyne in-phase and quadrature detection of weak coherent states with carrier phase tracking, J Sel Top Quantum Electron 15 (2009), 1581–1590.
14. J.A. López, A. Arvizu, E. García, F.J. Mendieta, E. Alvarez, and P. Gallion, Detection of phase-diffused weak coherent-states using an optical Costas loop, Opt Eng 51 (2012), 105002.
15. E. Desurvire, Classical and quantum information theory, Cambridge University Press, Cambridge, UK, 2009, pp. 691.
16. C.W. Helstrom, Quantum detection and estimation theory, Academic Press, New York, 1976, pp. 309.